

Sustainable and Green Corrosion Inhibition of Mild Steel: Insights from Electrochemical and Computational Approaches

Aicha Rizzi, Amel Sedik, Anissa Acidi, Khadidja Otmame Rachedi, Hana Ferkous,* Malika Berredjem, Amel Delimi, Amdjed Abdennouri, Manawwer ALAM, Barbara Ernst, and Yacine Benguerba*



Cite This: *ACS Omega* 2023, 8, 47224–47238



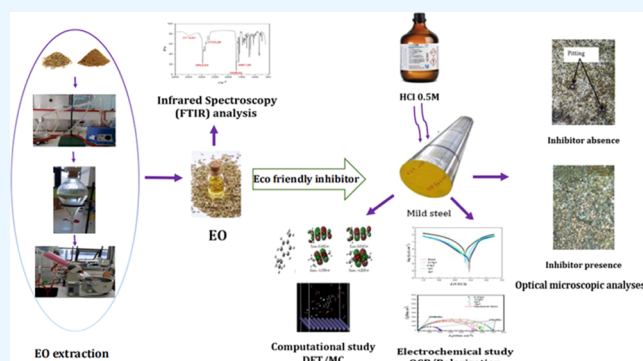
Read Online

ACCESS |

Metrics & More

Article Recommendations

ABSTRACT: Natural and fragrant compounds, essential oils (EOs) extracted from plants through hydrodistillation, are gaining popularity as eco-friendly and sustainable agents to protect metals and alloys from corrosion in acidic environments. This research focused on extracting and characterizing an EO obtained from the *Cuminum cyminum* (CC) plant native to India. The study aimed to evaluate the inhibitory properties of this EO on mild steel in a 0.5 M HCl solution at different concentrations. Various analytical techniques, including potentiodynamic polarization curves, electrochemical impedance spectroscopy, optical microscopy, infrared spectroscopy, and proton magnetic resonance, were employed to assess the effectiveness of this EO extract. Our findings indicate that the *Cuminum cyminum* L (CCL) extract effectively reduces the corrosion of mild steel in hydrochloric acid with an inhibition efficiency ranging from 79.69 to 98.76%. The optimal inhibition concentration was 2 g/L of EO, and surface analysis confirmed the formation of a protective layer. Furthermore, our results suggest that the inhibitor binds to the metal surface through a charge-transfer process, creating a protective film. Finally, we utilized theoretical calculations and molecular dynamics simulations to elucidate the inhibition mechanism on both a global and local scale.



1. INTRODUCTION

Steel is widely used in various industries, such as shipbuilding, petroleum, and construction, due to its availability, affordability, and strength.^{1–5} However, steel is highly susceptible to corrosion in acidic environments, leading to substantial financial losses for industries, estimated to be in billions of dollars annually.⁶ Acids are commonly used in industrial processes like petroleum refining, acid pickling, industrial cleaning, acid descaling, and petrochemical operations, exposing metals to corrosive agents.^{7,8} One frequently used industrial acid is hydrochloric acid, which corrodes metals through chemical or electrochemical reactions.^{9,10}

Over time, various methods have been developed to prevent or mitigate steel corrosion, including protective coatings, galvanization, cathodic protection, antirust solutions, and corrosion inhibitors.^{11–13} Corrosion inhibitors are substances added in small concentrations to corrosive environments to reduce or prevent metal reactions with their surroundings.^{14–16}

In aggressive industrial settings, corrosion inhibitors have proven highly effective in safeguarding metals from deterioration.^{17,18} These inhibitors attach themselves to the metal surface through specific interactions, primarily involving conjugated double bonds or atomic rings, nitrogen, sulfur, and oxygen heteroatoms, contributing to their strong corrosion

inhibition capabilities.^{19–21} Nevertheless, the widespread use and improper disposal of corrosion inhibitors have raised concerns about their potential harm to the environment and human health. Corrosion inhibitors can cause temporary or permanent damage to specific organs like the kidneys or liver and disrupt the body's enzyme systems.^{22–24} Adopting eco-friendly or green inhibitors offers a promising approach to reducing corrosion rates while minimizing environmental and health impacts.^{25–27} These inhibitors are typically derived from natural sources, such as essential oils (EOs) extracted from various plants, and are regarded as environmentally friendly and cost-effective.

Essential oils (EOs) are highly concentrated, hydrophobic liquids that capture the essence of the plant materials from which they are extracted.^{28,29} They are valued for their numerous beneficial biological properties, including antibacterial, antiviral, antifungal, antiparasitic, insecticidal, and

Received: September 26, 2023

Revised: November 15, 2023

Accepted: November 16, 2023

Published: December 1, 2023



antioxidant activities. EOs can be obtained through various methods such as steam extraction, dry distillation, and mechanical extraction. Their nontoxic and biodegradable nature makes them a promising candidate for use as corrosion inhibitors in harsh environments, including hydrochloric acid. EOs have effectively protected metals like copper and aluminum from corrosion.^{30–42}

Recent research has focused on the ability of EOs to prevent steel corrosion in hydrochloric acid.^{43–48} For example, *Citrus sinensis* EO was found to be an effective inhibitor against the corrosion of ordinary carbon steel in both 0.5 M H₂SO₄ and 0.5 M HCl solutions, with an optimal inhibition rate of 81.61% in HCl and 76.95% in H₂SO₄.^{43,44} Nutmeg EO was also an excellent inhibitor for carbon steel corrosion in a 1.0 M HCl solution, with an inhibition efficacy reaching up to 94.73% at 500 ppm of nutmeg oil.³⁸ The EO of caraway seeds (*Carum carvi* L) was used to protect carbon steel in a 1 M HCl solution, reaching a maximum efficiency of 94% at a concentration of 1 g/L.

EOs form a protective layer of adsorbed molecules on metal surfaces, inhibiting oxidation reactions and making them an effective solution for developing green inhibitors.^{49–52} Terpene-based chemicals derived from plant extracts are effective corrosion inhibitors in acidic media, with an inhibition efficiency ranging between 60 and 80% and the inhibition mechanism reported as mixed type or cathodic. Most cathodic terpene inhibitors were reported to chemisorb on the metal surface.^{53,54} The EO of *Ammodaucus leucotrichus* was studied by Manssouri et al. using electrochemical characterization and theoretical investigations. The inhibitory effect increased with the inhibitor concentration and the temperature, with quantum chemical calculations by density functional theory (DFT) and ELF analyses coherent with experimental findings.⁴⁰ *Artemisia Mesatlantica* EO was found to be an efficient inhibitor against carbon steel corrosion in 1 M HCl, with an inhibition efficiency reaching 92% at 3 g/L. The inhibition mechanism was a mixed type, and adsorption of the EO on the steel surface followed Langmuir's isotherm. The inhibitive layer was composed of an iron oxide/hydroxide mixture where the EO molecules were incorporated, as determined by scanning electron microscopy (SEM) and X-ray photoelectron spectroscopy (XPS) analyses.⁴¹

The present study investigates the potential corrosion-inhibiting effect of the EO obtained from Cumin (CCL), an annual herbaceous plant from Egypt. It is the world's second most commonly used spice after black pepper. The Cumin EO contains a variety of chemical classes, including a fraction of oxygenated monoterpenes primarily represented by cuminaldehyde (14–50%) and monoterpene hydrocarbons composed of β -pinene (5–17%), p-cymene (9–47%), and γ -terpinene (18–29%) as reported in ref 48. It is not just the majority compound that is responsible for protecting the steel; terpenes are important compounds that can work in synergy with the aldehyde.^{55,56} The study comprises three main steps: (1) isolating the CCL molecules from Cumin through successive column chromatography, (2) assessing the corrosion-inhibiting effect of the extracted molecules on mild steel in a 0.5 M HCl solution using electrochemical techniques, and (3) exploring the interactions between CCL molecules and metal surfaces through computational calculations based on DFT and MC simulations.

2. EXPERIMENTAL SECTION

2.1. Preparation of Extracts. The extraction of Cumin EO was carried out through a systematic multistep process, beginning with hydrodistillation. Initially, 75 g of cumin powder was combined with 1.5 L of tap water in a balloon heater. The mixture was then boiled for a duration of 2 h, allowing the vapor to facilitate the release of the oil. After condensation and liquefaction, the essential oil (EO) was efficiently separated from water using a separatory funnel. To further extract the EO from the aqueous phase, diethyl ether, an organic solvent, was employed in a liquid–liquid separation process. The addition of sodium chloride rendered the EO components less soluble in water, resulting in the formation of two distinct phases with the EO concentrated in the upper phase. The aqueous phase was subsequently decanted, and any remaining moisture in the organic phase was removed by adding anhydrous sodium sulfate. The final purification step involved filtration using a filter paper to eliminate impurities. Ultimately, the ether was evaporated using a Rotavapor, yielding pure CCL's EO. In the study, the corrosive medium was a 0.5 M HCl acid solution prepared by diluting concentrated hydrochloric acid with distilled water. Various concentrations of the EO inhibitor (ranging from 0.15 to 2 g/L) were introduced into the corrosive medium solutions. The EO yield was quantified by calculating the percentage of EO mass in relation to the mass of the dried plant material

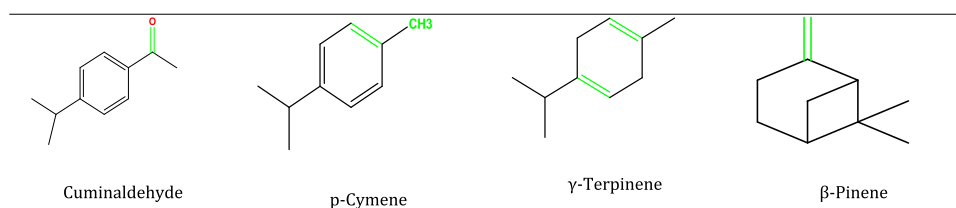
$$R_{\text{dtEO}} = \frac{M_{\text{go}}}{M_{\text{mv}}} \times 100 \quad (1)$$

where R_{dtEO} is the EO yield (%), M_{EO} is the mass of EO (g), and M_{mv} is the mass of dry plant matter (g).

To ensure accurate measurements, any free acids present in the EO were neutralized by using an ethanolic potassium hydroxide (KOH) solution. The analysis of the EO incorporated thin-layer chromatography (TLC) and column chromatography techniques for chromatographic analysis. TLC was used to enhance polarity and isolate the primary oil components based on their polarities, particularly focusing on the central part. Column chromatography was employed to purify individual components from the EO mixture, facilitating precise separation and purification. Following the isolation of individual components, the quantity of each pure fraction was determined, contributing to a comprehensive understanding of the EO's composition. Subsequently, infrared (IR) spectroscopic techniques were applied to ascertain the composition of these isolated components. IR spectroscopy provided crucial insights into the functional groups present in the compounds, aiding in their identification and characterization. The chromatographic analysis involved the use of a specific eluent composed of 95 mL of dichloromethane and 5 mL of petroleum ether during column chromatography. This selective eluent choice streamlined the separation and purification process.

2.2. Medium and Material. In this study, we explored the corrosion behavior of carbon steel, which was explicitly sourced from Arcelor Mittal in Algeria. The steel's chemical composition was determined to be 0.38% carbon, 0.27% silicon, 0.66% manganese, 0.02% nickel, 0.21% chromium, and 0.02% molybdenum, with the remaining composition consisting of iron (Fe). To inhibit corrosion, we employed varying concentrations of CCL's essential cumin oil, specifically at doses of 0.15, 0.5, 1, and 2 g/L. For the electrochemical tests,

Table 1. List of Significant Components of EOs Obtained from CCL



we utilized a standard three-electrode system with a Gamry reference 1000 potentiostat/galvanostat device and the Gamry Framework software. The electrode configuration included a saturated calomel (SCE) reference electrode from a Radiometer, a Ag/AgCl/KCl(sat) electrode maintained at a potential of +0.241 V relative to the standard hydrogen electrode, and a platinum (Pt) auxiliary electrode. The Pt electrode underwent a preparation process, which involved polishing with emery sheets of various grain sizes, followed by a final polishing step using 0.3 μm of diamond paste. Subsequently, the electrode was degreased with acetone, rinsed with distilled water, and dried using compressed air. To conduct the corrosion inhibition experiments, steel samples were immersed in a 0.5 M HCl solution containing varying quantities of essential cumin oil for 30 min. Tafel polarization curves were then generated in a potentiodynamic mode, encompassing both anodic and cathodic branches. These curves covered a potential range from −1000 to +600 mV/ECS at a scan rate of 1 mV/s. The selection of this scan rate was made to ensure that a stable state was reached without causing alterations to the environment that could potentially affect the electrode surface.

Additionally, electrochemical impedance diagrams were generated at a constant temperature of 25 °C, employing an amplitude of 10 mV and a frequency range spanning from 100 kHz to 10 mHz. All experiments were conducted under consistent ambient conditions to ensure valid comparisons. Essential electrochemical parameters, such as the corrosion potential (E_{corr}), polarization resistance (RP), corrosion current density (i_{corr}), cathodic (b_c), and anodic (b_a) Tafel slopes, as well as the inhibition rate, were calculated based on the current–potential curves obtained under realistic conditions.

2.3. Surface Characterization. Optical microscopy analysis was conducted to assess the morphology of the steel surface following a 30 min immersion in a 0.5 M HCl solution, both in the presence and absence of EO at the optimal concentration. The analysis was conducted at room temperature using a Nikon Eclipse LV150N microscope. The objective of this analysis was to ascertain whether the inhibition of corrosion could be attributed to the formation of a film of organic molecules on the steel surface.

2.4. Quantum Chemical Calculations and Molecular Dynamics Simulation. To identify the substances or molecules capable of effectively preventing steel corrosion in hydrochloric acid, we conducted a theoretical investigation using classical quantum mechanics methods and advanced theoretical approaches within the field of solid-state science and materials chemistry, particularly in the context of corrosion processes.⁵⁷ Specifically, we employed the density functional theory (DFT) technique to scrutinize the reaction mechanisms of organic inhibitors at the metal/solution interface. The primary components of the essential oils (EOs) obtained from CCL were analyzed in both their neutral and protonated forms

using the Gaussian 09 program with the B3LYP/6-31G(d,p) method.⁵⁸

The overall reactivity of the test molecules is closely tied to the presence of the frontier molecular orbitals, particularly the highest occupied molecular orbital (HOMO) and the lowest unoccupied molecular orbital (LUMO), within their electronic structures.⁵⁹ Furthermore, DFT facilitated the identification of various quantum chemistry parameters, including the electron affinity, hardness, chemical electronegativity, fraction of transferred electrons, and energy gap, offering a comprehensive overview of the chemical selectivity of the investigated inhibitors. Formulas for calculating these parameters can be found in the existing literature.^{60–62}

We assessed the local reactivity of organic inhibitors at the metal surface and evaluated them using a Fukui function population analysis. This analysis revealed both nucleophilic and electrophilic behaviors, shedding light on the reactive regions of the inhibitory compounds. Fukui function population analysis was also instrumental in detecting atomic charges and probing the internal reactivity of the inhibitors at various potential interaction sites with the metal surface.⁶³ Following the preparative thin-layer chromatography (TLC) process of the EO under study, four spots corresponding to the primary chemicals were distinguished (as detailed in Table 1). Theoretical investigations and quantum mechanics methods, such as DFT and Fukui function population analysis, provide invaluable insights into the reactivity and selectivity of potential inhibitors for preventing steel corrosion in aggressive environments like hydrochloric acid.

The Fukui function is defined as the first derivative of the electronic density concerning the number of electrons (N) while keeping an external potential $v(r)$ constant.⁶³ It is a valuable tool for exploring the reactivity and selectivity of molecules and materials and predicting the sites where chemical reactions are likely to occur, whether they are electrophilic or nucleophilic. The Fukui function is a central concept in theoretical chemistry and finds wide application in studying chemical reactivity and catalysis, spanning various fields, including materials science, organic chemistry, biochemistry, and surface science. Its computation involves a deep understanding of quantum mechanics and electronic structure theory,^{54,64} making it a potent instrument for investigating the reactivity and selectivity of complex materials and systems.

2.5. Monte Carlo Simulation. Monte Carlo simulation is a computational technique that leverages random sampling to investigate the behavior of complex systems. In the realm of materials science, Monte Carlo simulation finds application in the study of molecular adsorption on surfaces. One notable software tool for this purpose is the Adsorption Locator, which is available within Materials Studio. This tool empowers users to conduct Monte Carlo simulations of adsorption processes on surfaces by allowing them to specify various simulation parameters, including temperature, pressure, gas-phase compo-

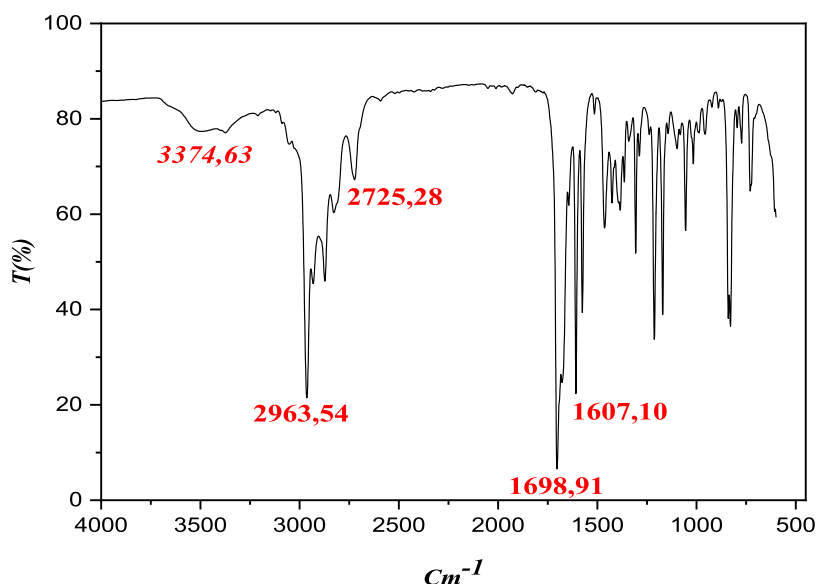


Figure 1. FTIR spectra of CCL EO.

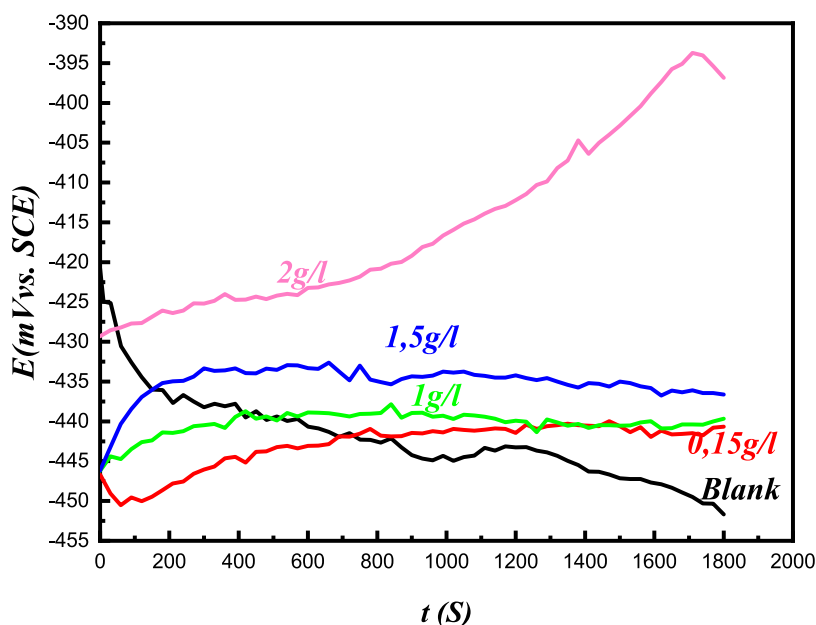


Figure 2. Time–potential curves for mild steel in a 0.5 M HCl solution, with and without various concentrations of EO from CCL, at 25 ± 1 °C.

sition, and surface properties. During the simulation, the program randomly places adsorbate molecules on the surface and computes the system's energy. This energy is determined by the interactions among the adsorbate molecules and between the adsorbate molecules and the surface. The simulation then aims to rearrange the adsorbate molecules on the surface in accordance with the principles of thermodynamics, followed by a recalculation of the system's energy. The acceptance of the new configuration is determined by changes in energy and the system's temperature using the Metropolis algorithm. Through the iterative simulation of numerous steps, the program generates a distribution of adsorption configurations that adhere to predefined conditions. Subsequently, these configurations can be analyzed to derive essential thermodynamic and kinetic characteristics of the adsorption process such as the adsorption isotherm, heat of adsorption, and diffusion coefficient. When executed under the

specified conditions within the Adsorption Locator tool of Materials Studio software, Monte Carlo simulation becomes a powerful instrument for gaining insights into how molecules interact with surfaces. This approach offers valuable insights into the design of novel materials with applications spanning a wide range of industries and contexts.

3. RESULTS AND DISCUSSION

3.1. Fourier Transform Infrared (FTIR) Spectroscopy Analysis. Fourier transform infrared (FTIR) spectroscopy serves as a potent analytical technique employed to investigate the chemical composition of various substances, including essential oils. This methodology proves instrumental in identifying the specific functional groups within essential oils, which are complex mixtures encompassing various organic compounds such as terpenes, alcohols, esters, and phenols. These functional groups play a pivotal role in influencing the

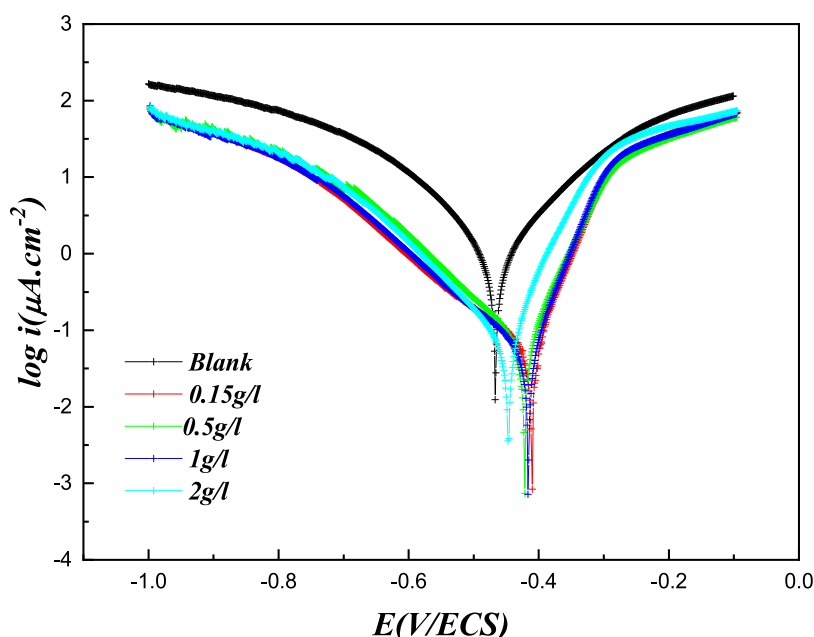


Figure 3. Polarization curves in a 0.5 M HCl solution containing different concentrations of EO of CCL.

reactivity and effectiveness of these compounds as corrosion inhibitors. In particular, certain functional groups possess the ability to form protective layers on metal surfaces, which is a crucial mechanism in the inhibition of corrosion. The primary aim of this analysis is to gather crucial insights into the chemical constituents of essential oils and how these constituents correlate with the potential of oils as corrosion inhibitors. In our specific case, the most prevalent functional groups identified are the carbonyl functions (C=O) and C–H bonds, indicative of the presence of cuminaldehyde, a finding supported by the existing literature. Furthermore, we observed vibrations associated with the C=C function, characteristic of terpenes such as β -pinene, p-cymene, and γ -terpinene.⁴⁸ The functional groups present in the essential oil obtained from CCL were identified through an analysis of the FTIR (Fourier transform infrared) spectrum, which provides valuable information regarding the absorbance bands linked to various constituents (see Figure 1). Given the abundance of cuminaldehyde and terpene compounds in the oil, the spectrum revealed prominent absorbance bands at specific wavenumbers: an absorbance band at 1607.10 cm^{-1} , signifying the presence of carbonyl groups (C=O) within the compounds; another significant absorbance band at 1698.91 cm^{-1} indicates unsaturation (C=C) in the molecular structure; an absorbance peak at 2725.28 cm^{-1} attributed to the C–H (carbon–hydrogen) bond within the aldehyde functional group; The spectrum also exhibited a notable band at 2963.54 cm^{-1} , indicative of aromatic C–H bonds; and an absorbance band at 3374.63 cm^{-1} was observed, corresponding to the O–H (hydroxyl) functional group.

These absorbance bands observed in the FTIR spectrum provide invaluable information concerning the chemical composition and functional groups present in the essential oil from CCL, facilitating the identification of its constituent elements.

3.2. Corrosion Study. **3.2.1. Open Circuit Potential (OCP).** Reliable electrochemical experiments require the establishment of steady-state open circuit condition. Changes in the open circuit potential (OCP) of mild steel over time

provide valuable insights into the onset and progression of corrosion.^{1,65} In this study, the E_{ocp} of mild steel was monitored for 30 min when exposed to the test solutions. Figure 2 illustrates the E_{ocp} of mild steel in the blank solution, showing a shift toward more favorable potentials due to the dissolution of active metals, such as Fe, in the HCl solution. After an initial period of exposure, the potential stabilizes. In the presence of CCL's essential oil (EO), the initial E_{ocp} becomes more cathodic compared to the acid solution without inhibitors. The most significant effect is observed at the lowest concentration, and E_{ocp} values transition from negative to positive as the EO concentration increases. This suggests that the EO influences the cathodic reaction. Upon immersing the electrode into the solution, the metal's E_{ocp} rapidly transitions toward passive regions. The inhibitor molecules adhere to the metal surface, expediting the approach to equilibrium. The inhibitor film exhibits high stability, particularly at higher concentrations.

3.2.2. Polarization Curves. One of the most widely used techniques for assessing electrochemical parameters is potentiodynamic polarization (PP). This technique involves sweeping the potential of the test electrode over a wide range, allowing for the generation of sufficient current to drive the oxidation and reduction reactions on the metal surface. The results are presented in the form of polarization curves, where the potential for each measured point is plotted against the corresponding current density (i) or $\log(i)$. Figure 3 displays the semilogarithmic potentiodynamic polarization curves of mild steel obtained in a 0.5 M HCl solution, both with and without varying concentrations of CCL's essential oils.

Upon close examination of these curves, it becomes evident that the addition of the inhibitor leads to a reduction in the anodic partial current, which corresponds to the dissolution of the metal, as described by the reaction



Furthermore, this decrease in the cathodic current results in reductions in the production of hydrogen and oxygen. The reduction reactions are represented by



In these reactions, the flow of electrons (e^-) at the cathode reduces either H^+ or O_2 , leading to the production of hydrogen gas (H_2) or hydroxide ions (OH^-), depending on the specific conditions. A decrease in the cathodic current indicates a reduced rate of these reduction reactions, ultimately resulting in decreased hydrogen and oxygen production. The inhibitory efficiency ($E\%$) is calculated using the following equation when considering various essential oil concentrations in a 0.5 M HCl medium at 25 °C

$$E(\%) = \left(\frac{i_{\text{corr}} - i'_{\text{corr}}}{i_{\text{corr}}} \right) \times 100 \quad (5)$$

The current density values for steel corrosion, represented as i_{corr} and i'_{corr} , are determined through the extrapolation of the Tafel lines. These extrapolations are carried out after immersing the steel in an acidic environment, both in the presence and absence of different concentrations of corrosion inhibitors. The observed results are summarized in Table 2.

Table 2. Electrochemical Impedance Characteristics in the Absence and Presence of Various EO Concentrations

C (g/L)	E_{corr} (mV/ECS)	i_{corr} ($\mu\text{A}/\text{cm}^{-2}$)	R_{p} ($\Omega \cdot \text{cm}^2$)	b_{a} (mV)	b_{c} (mV)	E (%)
SI	-472.08	567.13	46.9	110.5	137.2	-
0.15	-433.00	75.65	129.4	55.8	167.1	86.66
0.5	-432.15	15.67	240.0	44.3	186.1	97.23
1	-403.41	10.492	1032.0	40.4	137.6	98.15
2	-419.94	1.64	7939.0	46.0	86.3	99.71

Based on the data presented in Figure 3, within a corrosive solution lacking the extract, the corrosion potential of mild steel (MS) measures at -0.474 V when compared to the Ag/AgCl reference electrode. As the potential shifts toward anodic or cathodic overpotentials, both anodic and cathodic current densities increase, a phenomenon primarily governed by activation processes.⁶⁶ However, when the corrosive medium is treated with the EO of CCL, several significant effects become apparent. The cathodic potential of the medium increases, resulting in a simultaneous reduction in both anodic and cathodic current densities.⁶⁷

The EO of CCL demonstrates noteworthy effectiveness in slowing the rate of anodic metal dissolution and the rate of cathodic hydrogen gas evolution. The variation in the corrosion potential is less than 85 mV, contingent on the inhibitor concentration. Both anodic and cathodic partial currents decrease, signifying the mixed nature of the inhibitor and its capacity to diminish the rate of anodic steel dissolution and the rate of H^+ proton reduction and oxygen reduction.^{2,68} With an increase in the inhibitor concentration, the current density experiences a substantial decline. For instance, at a concentration of 0.15g/L of Cumin EO, the current density decreases to $75.65 \mu\text{A}/\text{cm}^{-2}$, and at 2 g/L of the inhibitor, it further diminishes to $1.64 \mu\text{A}/\text{cm}^{-2}$, in comparison to the $567.193 \mu\text{A}/\text{cm}^{-2}$ observed in the absence of the inhibitor. In the cathodic domain, the addition of Cumin EO leads to slight alterations in the cathodic Tafel slopes (b_{c}), indicating that the reduction of H^+ protons at the steel surface remains unaffected

by the inhibitor, progressing based on a pure activation mechanism.⁶⁹

Furthermore, as the inhibitor concentration increases, the polarization resistance significantly increases, ranging from 46.9 to 7939 $\Omega \cdot \text{cm}^2$ at a concentration of 2 g/L. The inhibitory efficiency ($E\%$) also demonstrates an upward trend with increasing inhibitor concentration, reaching a peak of 99.71% at 2 g/L of Cumin EO.

These findings unequivocally suggest that inhibition efficiency experiences a sharp ascent with an increase in concentration, achieving a practical level of inhibition at approximately 0.5 g/L. This phenomenon is attributed to the adsorption mechanism and surface processes. Higher inhibitor concentrations result in greater availability of inhibitor molecules, leading to more extensive surface coverage. Additionally, employing Cumin EO as an inhibitor provides advantages due to its natural and cost-effective properties. Consequently, if the EO of CCL is readily accessible, it may be a viable alternative in the metal industry.

3.2.3. Electrochemical Impedance Spectroscopy. Electrochemical impedance spectroscopy (EIS) has recently gained popularity due to its capacity to offer valuable insights into the physical and electronic properties of electrochemical systems. This method is particularly reliable because it does not significantly polarize the metal and does not alter the interaction between the metal and the solution. The resulting curves provide crucial information about the underlying mechanisms of surface reactions, making EIS particularly useful in corrosion inhibition studies. Therefore, in this study, EIS was employed to investigate the inhibitory effects of the compound. Figure 4 displays the Nyquist plots of the electrode immersed in a 0.5 M HCl solution, in both the absence and presence of various concentrations of CCL EO.

The EIS data were analyzed by fitting the experimental data using EC-LAB software, and the results are presented in Table 4. To achieve this objective, two electrical equivalent circuit diagrams are provided in Figure 5.

In Figure 4a, the Nyquist plots clearly exhibit a capacitive loop at high frequencies, followed by an inductive arc at low frequencies in the absence of the inhibitor and with low inhibitor concentrations. The capacitive loop observed at high frequencies is associated with the double electric layer phenomenon, arising from charge transfer in the corrosion process as well as double-layer resistance and film resistance.

Conversely, the low inductive loop indicates relaxation of species from the surface and the presence of unstable corrosion products at the metal surface.^{1,2,25,70} In the presence of the essential oil of LCC, the inductive loop at low frequencies disappears, and a single depressed capacitive semicircular shape emerges.⁷¹ This change indicates that the rate of mild steel dissolution in the HCl solution, in the presence of the inhibitor, is primarily controlled by a charge-transfer process. Furthermore, the capacitive loops in these conditions are slightly depressed and take the form of semicircles with a center below the real axis. This distortion is attributed to frequency dispersion caused by the adsorption of inhibitor molecules at the metal surface, the formation of a porous layer, and the heterogeneity of the electrode surface.⁷²⁻⁷⁴ The diameter of the Nyquist plots, which represents the corrosion protection ability of the inhibitor, increases as the concentration of LCC EO increases. This observation confirms that the inhibition of LCC EO on the corrosion of mild steel in a 0.5 M HCl solution occurs through the adsorption of the

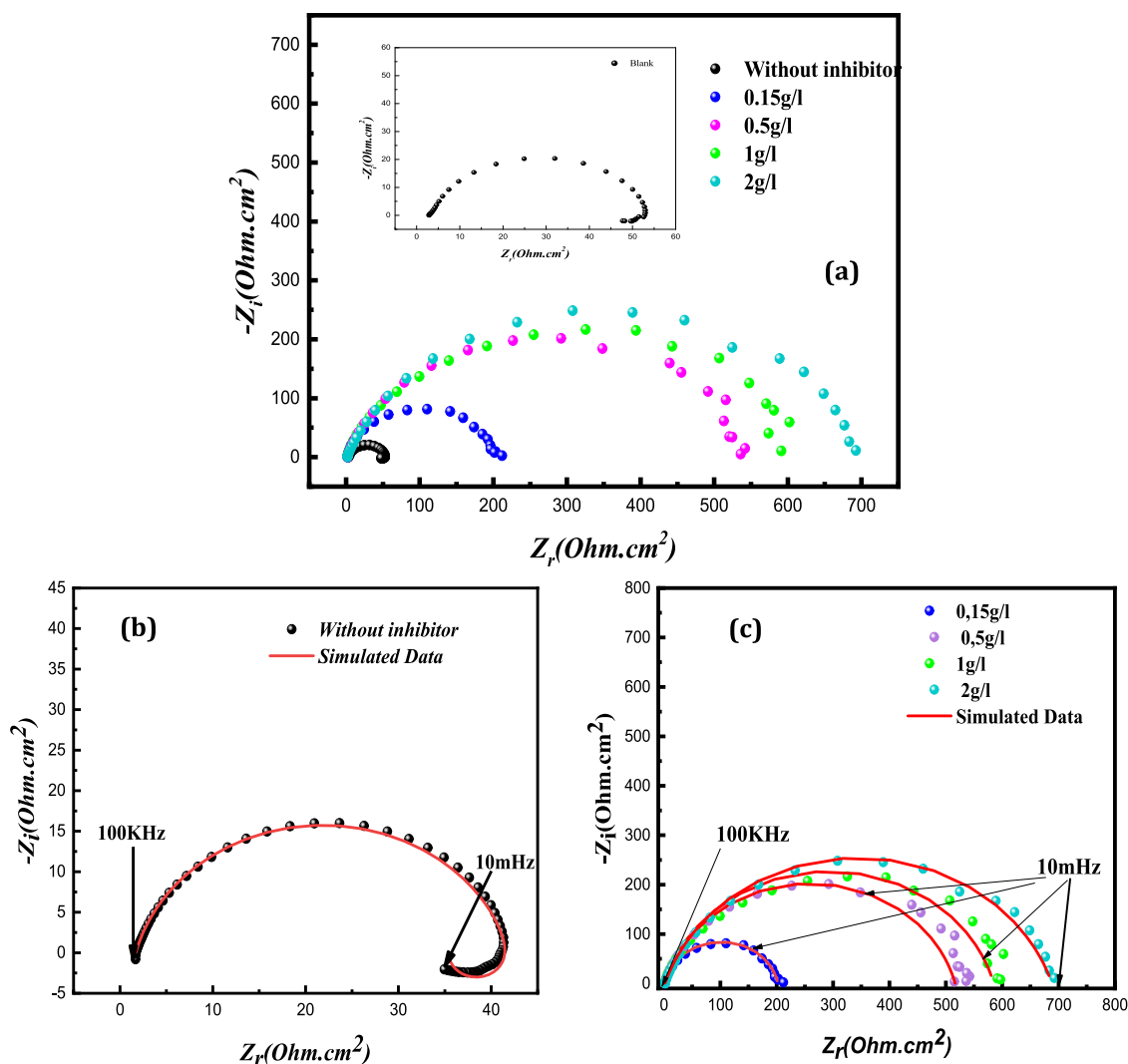


Figure 4. Electrochemical impedance diagrams in Nyquist representation (a) and simulated curves of steel in HCl at 0.5 M without (b) and with (c) different concentrations of the EO of CCL after 30 min of immersion.

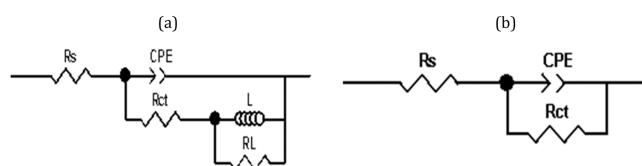


Figure 5. Equivalent steel electric circuit in 0.5 M HCl in the absence (a) and presence (b) of different concentrations of Cumin EO.

inhibitor molecules and is attributed to the formation of a $[\text{Fe-Inh}]^{2+}$ film.

The presence of the initial capacitive semicircle indicates that the corrosion reaction in the free-flowing 0.5 M HCl solution is primarily controlled by charge transfer (R_{ct}). This first capacitive loop signifies that the corrosion process of mild steel (MS) occurs in a 0.5 M HCl solution under activation control. Additionally, the capacitive semicircle is associated with the diffuse layer resistance (R_d) and accumulation resistance at the steel/solution interface (R_a), which collectively creates a barrier effect. The summation of these resistances represents the polarization resistance (R_p), as follows

$$R_p = R_{ct} + R_d + R_a \quad (6)$$

This description pertains to the system's behavior in the absence of an inhibitor. At low frequencies, the appearance of an inductive loop (RL) may be attributed to the relaxation process on the metal surface or the presence of unstable corrosion products at the metal/solution interface, such as FeCl_2 .^{8,75} The inductive loop suggests that the soluble corrosion products do not effectively adhere to the metal surface. Such systems can be explained in terms of electrical circuits that involve inductance elements.^{76,77}

To model the various processes taking place at the interface between the electrode and electrolyte, an equivalent electrical circuit (EEC) is employed. Two EECs are presented: one without an inhibitor and the other with an EO of CCL at various concentrations. In these circuits, each component represents a specific physical parameter and may be interconnected in series or parallel. These models are refined iteratively to closely match the experimental impedance diagrams, enabling the extraction of parameters necessary for a comprehensive understanding of the system under investigation. Figure 5 depicts the EEC constructed using the EC-lab simulation software. The electrical circuit comprises

several elements including an electrolyte resistor (R_s), a charge-transfer resistor (R_{ct}), and a constant phase element (CPE). The CPE is utilized instead of a double-layer capacitance (C_{dl}) to account for surface area heterogeneities.⁷⁸ This circuit has proven to be effective in accurately replicating real-world conditions. The results of the parameter tuning process and the calculated inhibitory effectiveness, using eq 3,

Table 3. Electrochemical Parameters Derived from the Electrical Circuit of Steel in 0.5 M HCl in the Absence and Presence of the Inhibitor, as well as the Inhibitory Efficiencies

	R_s	CPE ($10^{-6}/s^n \Omega^{-1}\cdot\text{cm}^{-2}$)	R_p ($\Omega\cdot\text{cm}^2$)	E(%)
SI	1.60	757.95	41.50	-
0.15 g/L	1.64	68.02	204.4	79.69
0.5 g/L	1.95	34.99	531.0	93.15
1 g/L	2.00	29.70	605.9	97.96
2 g/L	1.83	26.78	974.3	98.76

are summarized in Table 3, along with their respective parameter values

$$E(\%) = \left(\frac{R_p' - R_p}{R_p'} \right) \times 100 \quad (7)$$

where R_p and R_p' represent the charge-transfer resistances in the absence and presence of the inhibitor, respectively. Table 3 displays the electrochemical parameters derived from the electrical circuit of steel in a 0.5 M HCl solution in the absence and presence of the inhibitor as well as the inhibitory efficiencies.

As observed in the table, the presence of the inhibitor leads to a decrease in the double-layer capacitance (CPE) values and an increase in polarization resistance (R_p). This decline in the CPE value can be attributed to the adsorption of inhibitor molecules onto the steel surface, creating a barrier. To provide an electrical analogy, imagine a capacitor with a double layer formed at the interface between the electrode and the solution. When Cumin EO molecules displace water molecules in the electrolyte adsorbed on the steel surface, the capacitance of the capacitor decreases.^{2,79} An increased inhibitor adsorption results in a thicker organic deposit and a lower double-layer capacity. The inhibitory efficiency is positively correlated with the inhibitor concentration, with the highest efficiency reaching 99.40% at 2 g/L.

3.2.4. Steel Surface Analysis by Optical Microscope. Following a 30 min immersion of the steel surface in 0.5 M HCl at room temperature, in both the presence and absence of CCL EO at a concentration of 2 g/L, a surface analysis was conducted. In the absence of an inhibitor, as depicted in Figure 6, the steel surface displays damage characterized by the development of pitting. These pits result from the dissolution of iron in the hydrochloric medium, indicating widespread pitting corrosion across the entire steel surface. These findings are further supported by three-dimensional (3D) micrography.

Figure 7 presents the steel surface after undergoing the same immersion duration in the presence of EO. When an inhibitor concentration of 2 g/L is used, a noticeable reduction in pits on the sample's surface is observed. This reduction suggests that molecules from Cumin EO adsorb and form a protective layer over the surface. Upon microscopic examination of the steel treated solely with acid, a thin film is discernible, covering its surface. This observation confirms that inhibition occurs because the electrolyte cannot access the steel's surface due to the formation of a cohesive, solid, and insoluble coating.

The key components of Cumin EO, including cuminaldehyde, p-cymene, γ -terpinene, and β -pinene, play a pivotal role in creating a protective layer on the steel surface. This protective film adheres to the steel by interacting with various electron functionalities. For instance, the nonbonding electrons associated with the carbonyl function of cuminaldehyde, as well as the double bonds present in this compound and the terpenes (p-cymene, γ -terpinene, and β -pinene), participate in the formation of chemical bonds, leading to the establishment of dative bonds with the steel.

3.3. Theoretical Chemical Calculation. **3.3.1. Reactivity Analysis of the Inhibitor Molecules.** Using DFT B3LYP/6-31G(d,p) calculations in both a vacuum and DMSO (dimethyl sulfoxide) solvent, we determined several vital parameters including electronegativity (χ), maximum transferred electron fraction (ΔN_{max}), electron potential (μ), hardness (η), molecular softness (S), and the electrophilicity index (ω). The equations used to compute these parameters can be found in Table 4. These parameter values provide valuable insights into the stability and reactivity of the molecules.^{80,81}

Table 5 displays four major molecules' optimized minimum energy geometrical configurations in CCL's EO, specifically cuminaldehyde, p-cymene, γ -terpinene, and β -pinene.

The molecular orbitals HOMO and LUMO provide valuable insights into the regions or sites where electron donation or acceptance is likely to occur. The distribution of molecular orbitals reveals that in DMSO, compound (a) exhibits a wide

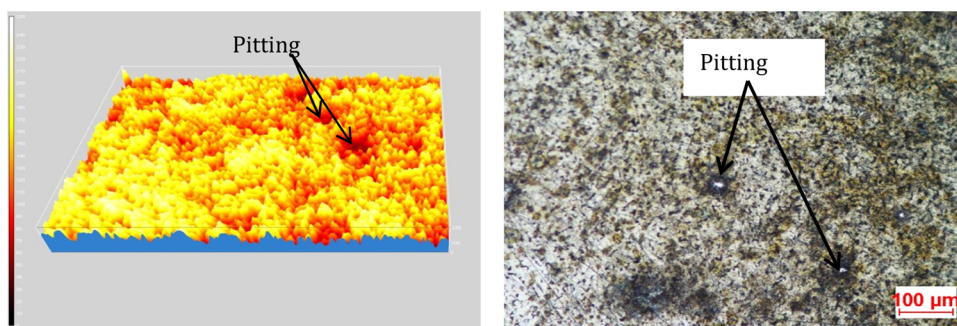


Figure 6. Micrograph obtained by optical microscopy in 2D and 3D of the steel in 0.5 M HCl in the absence of the EO of CCL after 30 min of immersion.

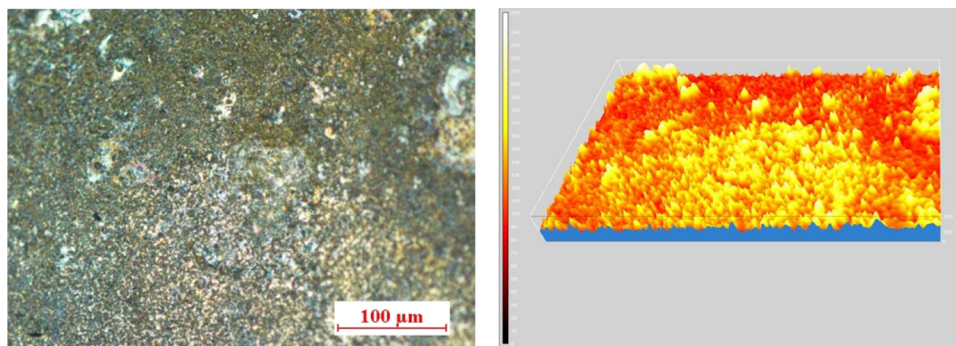


Figure 7. Micrograph obtained by optical microscopy in 2D and 3D of the steel in 0.5 M HCl in the presence of the EO of CCL after 30 min of immersion.

Table 4. Global Reactivity Parameter Equations

parameters	eqs
ionization energy	$I = -E_{\text{HOMO}}$
electronic affinity	$A = -E_{\text{LUMO}}$
electronegativity	$\chi = -(E_{\text{HOMO}} + E_{\text{LUMO}})/2$
electronic chemical potential	$\mu = -\chi = (E_{\text{HOMO}} + E_{\text{LUMO}})/2$
chemical hardness	$\eta = (E_{\text{LUMO}} - E_{\text{HOMO}})/2$
electrophilicity index	$\omega = \mu^2/2\eta$
molecular softness	$S = 1/\eta$
maximum transferred electron fraction	$\Delta N_{\text{max}} = -\mu/\eta$

distribution of HOMO and LUMO orbitals throughout the molecule, indicating a high level of reactivity. In a vacuum, compound (b) displays HOMO and LUMO orbitals distributed throughout the molecule. A higher E_{HOMO} value implies a better ability of inhibitor molecules to donate electrons to the vacant orbitals of the metal atom. Conversely, a lower E_{LUMO} value suggests a better ability of the inhibitor to accept electrons from the filled orbitals of the metal through a back-donation mechanism. The energy gap ΔE is commonly employed to assess the relative reactivity of inhibitor molecules with the metal atom. A lower value of ΔE implies better inhibition efficiency, while a higher value indicates a lower inhibition efficiency. Figure 8 visually represents the optimized minimum energy geometrical configurations of four major molecules found in the CCL's EO: cuminaldehyde, p-cymene, γ -terpinene, and β -pinene, along with their corresponding descriptor values.

In a vacuum, p-cymene has the lowest hardness value and highest electrophilicity and ΔN_{max} values, indicating that it is a good electrophile and more susceptible to nucleophilic attacks (Table 6). On the other hand, in DMSO, cuminaldehyde has the lowest hardness value and highest electrophilicity and ΔN_{max} values, making it the most reactive molecule and susceptible to nucleophilic attacks. These results suggest that both compounds have the potential as inhibitors for corrosion

protection of steel in different environments, with p-cymene being more effective in a vacuum and cuminaldehyde being more effective in DMSO.

The Fukui functions offer valuable insights into a molecule's reactivity concerning nucleophilic or electrophilic interactions. Specifically, the f^+ function indicates the site at which the molecule is most susceptible to an electrophilic attack. Conversely, the f^- function signifies the site where the molecule is most prone to a nucleophilic attack. The f^0 function designates the area where the molecule undergoes a reaction without altering its electronic density.^{82,83}

The following equations calculate the Fukui functions

$$f^+(i) = n(i+1) - n(i) \quad (8)$$

$$f^-(i) = n(i) - n(i-1) \quad (9)$$

$$f^0(i) = (1/2)[f^+(i) + f^-(i)] \quad (10)$$

where $n(i)$ is the total electron density in the i th state, and $i-1$, i , and $i+1$ are the states where the electron density changes due to the addition or removal of an electron.

The Fukui function values for each molecule in vacuum and DMSO are presented in Table 7. The values of f^+ and f^- functions suggest that the most reactive sites in all molecules in a vacuum are located in the terpenes, mainly in the p-cymene molecule (b). In contrast, DMSO's most reactive site is situated in the cuminaldehyde (a) carbonyl group, consistent with the previous reactivity results.

The local electrophilicity ω_k^+ is defined by $\omega_k^+ = \omega f^+$,⁸⁴ where ω^+ is the local electrophilicity index and f^+ is the Fukui index of nucleophilic attacks.

We can pinpoint the most reactive sites in the studied compounds by analyzing the Fukui index values. In compound (a), the carbonyl group of the (C10) and (O11) atoms stands out as the most reactive site, displaying a high susceptibility to nucleophilic and electrophilic attacks, respectively. Moving on to compound (b), the carbon atom (C5) emerges as the

Table 5. Calculated Parameters of Studied Molecules Obtained by B3LYP/6-31G (d, p) in Vacuum and DMSO

descriptor	vacuum				DMSO			
	a	b	C	d	a	b	c	d
α_{Tot} (Bohr ³)	108.01	103.25	103.38	100.04	137.58	133.96	134.27	132.43
E_{HOMO} (eV)	-6,7685	-6,1584	-5,9214	-6,2352	-6,9576	-6,2828	-5,9987	-6,3182
E_{LUMO} (eV)	0,4110	0,16027	0,8427	0,7797	-1,6615	0,0165	0,7545	0,68654
ΔE_{gap} (eV)	7,1795	<u>6,3187</u>	6,7641	7,0149	<u>5,2961</u>	6,2993	6,7532	7,0047
E (u.a)	-463,536	-389,531	-390,705	-390,678	-463,511	-389,534	-390,707	-390,679

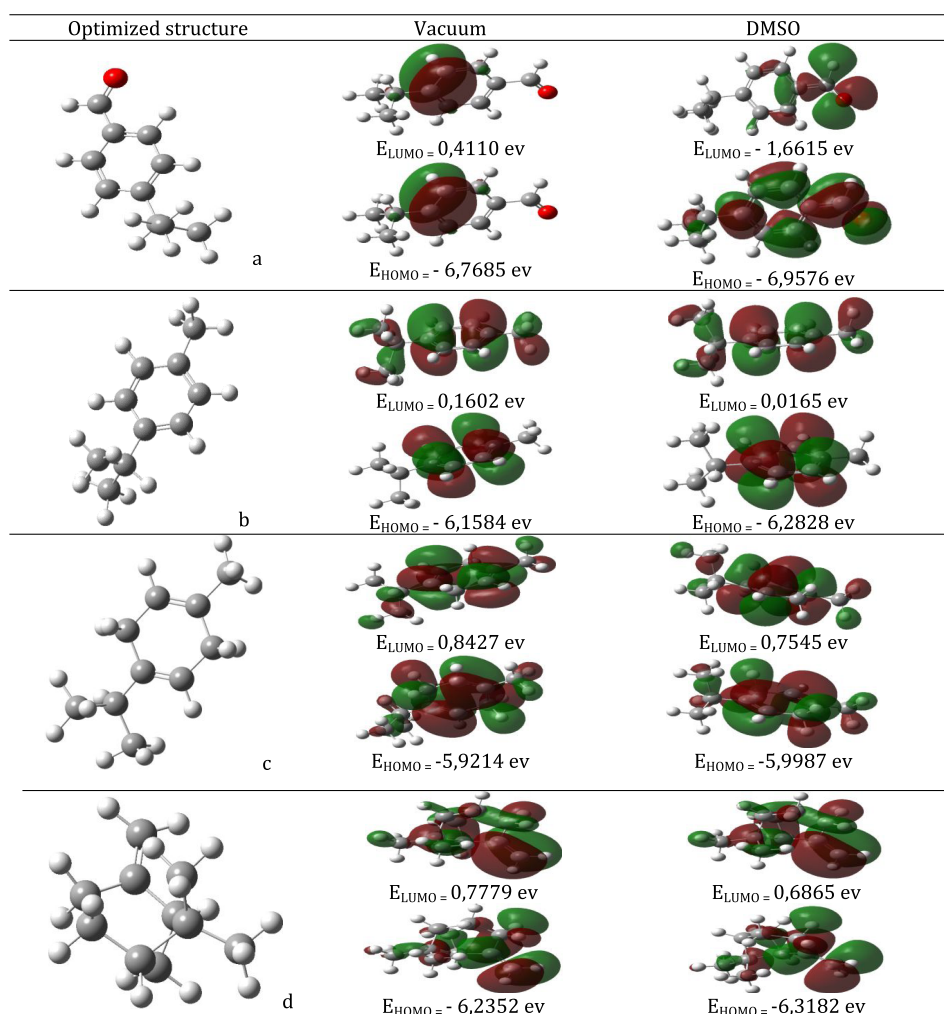


Figure 8. Optimized structure and molecular orbital (HOMO, LUMO) distributions of studied compounds in vacuum and DMSO obtained by B3LYP/6-31G (d,p).

Table 6. Reactivity Descriptors Are Calculated Values of Studied Compounds

	vacuum						DMSO					
	η	S	μ	X	ω	ΔN_{\max}	η	s	μ	X	ω	ΔN_{\max}
a	3,590	0,278	-3,179	3,179	1,407	0,886	2,648	0,378	-4,310	4,310	3,507	1,627
b	3,159	0,316	-2,999	2,999	1,423	0,949	3,150	0,317	-3,133	3,133	1,558	0,995
c	3,382	0,296	-2,539	2,539	0,953	0,751	3,377	0,296	-2,622	2,622	1,018	0,777
d	3,506	0,285	-2,728	2,728	1,061	0,778	3,502	0,285	-3,089	3,089	1,362	0,882

electrophilic site with a notably high f^+ value, while the carbon atom (C3) is identified as the nucleophilic site. Compound (c) exhibits the highest f^+ value in proximity to the carbon atom (C5), while the carbon atom (C6) boasts the highest f^- value, signifying their respective inclinations toward electrophilic and nucleophilic attacks. Lastly, examining compound (d), we find that the carbon atom (C7) serves as the most reactive site for electrophilic attacks, whereas the carbon atom (C6) is earmarked as the nucleophilic site. These findings provide valuable insights into the reactivity of the studied compounds and can assist corrosion science researchers in identifying potential attack sites within these molecules.

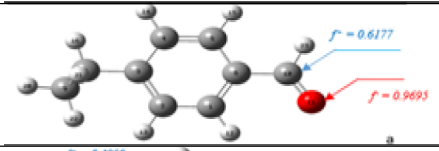
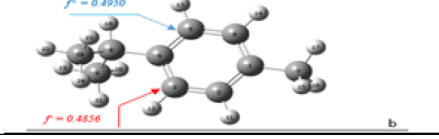
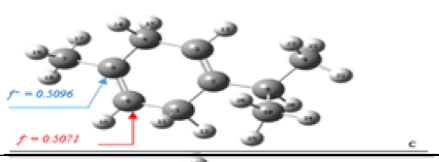
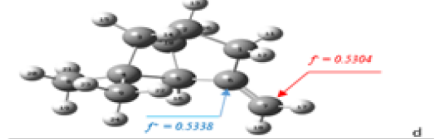
3.3.2. Molecular Electrostatic Potential (MESP). In corrosion science, the ability to predict molecular regions susceptible to electrophilic and nucleophilic attacks holds

significant importance. The molecular electrostatic potential (MESP) graphical map is a valuable tool (Figure 9).

In MESP diagrams, the red portions signify negative charges, while the blue areas denote positive charges. Green zones indicate intermediate potentials between the extremes, whereas yellow and light blue represent potentials between the middle and the extremes, respectively. Upon scrutinizing the MESP diagrams of these compounds, noteworthy observations can be made. In compound (a), the red regions on the MESP diagram are associated with the oxygen atom (O11). Likewise, for compounds (b) and (c), the red areas correspond to the carbon atoms in the cyclic parts, specifically (C1) and (C6), respectively. Finally, compound (d)'s red region is proximate to carbon (C7) in the MESP representation.

Table 8 provides insight into the specific regions of the studied compounds with the most substantial negative

Table 7. Local Reactivity Parameters of the Studied Molecules

	Atom	f	f^+	ω^+	ω^-	
a	C10	0.0228	0.6177	0.3814	0.0141	
	O11	<u>0.9695</u>	0.3683	0.2274	0.5987	
b	C2	0.0180	0.0011	0.0003	0.0049	
	C3	<u>0.4856</u>	0.0004	0.0001	0.1313	
	C4	0.4681	0.0107	0.0029	0.1265	
	C5	0.0150	<u>0.4950</u>	0.1338	0.0040	
	C6	0.0015	0.4829	0.1305	0.0004	
c	C1	0.0126	0.0057	0.0018	0.0040	
	C5	0.4633	<u>0.5096</u>	0.1632	0.1484	
	C6	<u>0.5071</u>	0.4694	0.1504	0.1625	
d	C6	0.4425	<u>0.5338</u>	0.1817	0.1506	
	C7	<u>0.5304</u>	0.4467	0.1520	0.1805	

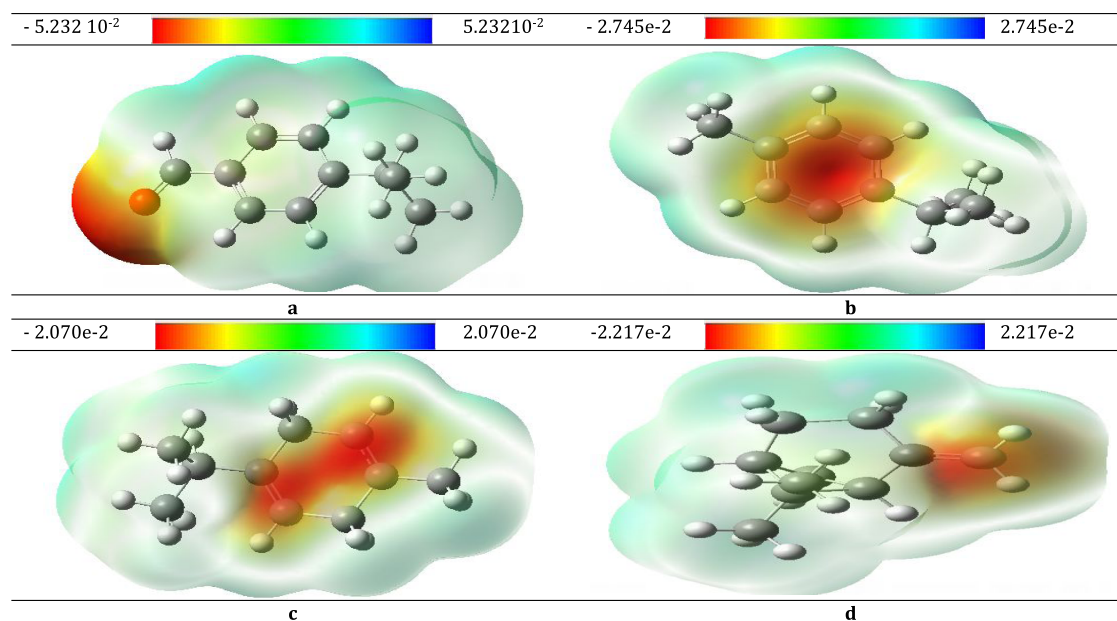


Figure 9. Molecular electrostatic potential map for studied compounds on total density: compound a (a), compound b (b), compound c(c), and compound d (d).

Table 8. Most Negative Potential Regions of the Studied Compounds

compound	element	negative potential region	region color
a	O11	-0.05227	red
b	C1	-0.02720	red
c	C6	-0.01925	red
d	C7	-0.02196	red

electrostatic potentials. In all four compounds (a–d), these regions are visually highlighted in red on the molecular electrostatic potential (MESP) diagrams. This information is valuable for understanding the areas of these molecules that are most susceptible to nucleophilic attacks. These negatively charged regions can act as electron-rich sites, making them

prone to reactions with electrophilic species, which is a crucial aspect of corrosion science research. Notably, these regions vary across the compounds, indicating distinct sites of reactivity within each molecule.

3.3.3. Monte Carlo Simulations. The investigation into the adsorption characteristics of these molecules on the iron surface (110) using Monte Carlo simulations in a water and HCl solvent environment yielded significant results, as summarized in Figure 10 and Table 9.

Table 9 provides insights into the inhibition system's adsorption energies (kcal/mol). These energies encompass various aspects, such as total energy, adsorption energy, rigid adsorption energy, deformation energy, and specific contributions from different molecular species such as β -pinene, H_2O , H_3O^+ , and Cl^- . The study's findings indicate that all four

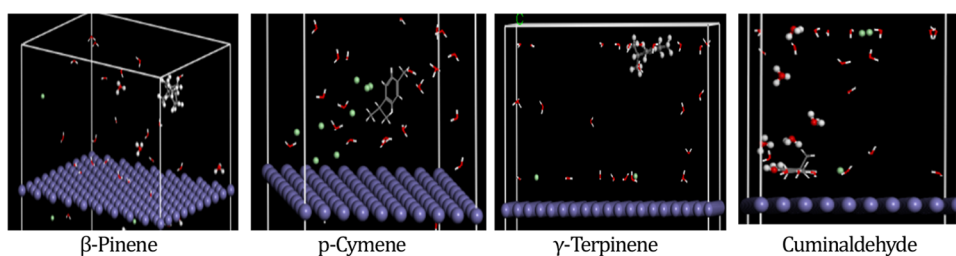


Figure 10. Equilibrium adsorption configurations of studied inhibitors on the iron(110) surface obtained by molecular dynamics simulations.

Table 9. Adsorption Energies (kcal·mol⁻¹) of the Inhibition System

	total energy	adsorption energy	rigid adsorption energy	deformation energy	β -pinene $\frac{dE_{ad}}{dN_i}$	H ₂ O $\frac{dE_{ad}}{dN_i}$	H ₃ O ⁺ $\frac{dE_{ad}}{dN_i}$	Cl ⁻ $\frac{dE_{ad}}{dN_i}$
β -pinene	-40.010	-6.901×10^4	-43.365	-6.897×10^4	-6.804×10^4	-11.393	-32.224	-0.565
p-cymene	-11.619	-5.318×10^6	-31.728	-5.318×10^{20}	-21.633	-10.794	-18.448	-5.318×10^{19}
γ -terpinene	-13.271	-1.054×10^3	-42.612	-1.012×10^3	-28.791	-11.370	-37.377	-0.882
cuminaldehyde	-8.038	-885.611	-39.046	-846.564	-41.995	-9.526	-20.028	-0.122

inhibitor molecules can effectively inhibit iron corrosion when exposed to an acidic aqueous solution. The negative values of adsorption energy (E_{ads}) suggest an exothermic and spontaneous adsorption process. This indicates the formation of stable and strong bonds between the inhibitors and the Fe(110) surface. Consequently, this bond strengthens the surface, making it more resistant to attack by corrosive agents. Notably, the absolute value of E_{ads} measures the bond strength between the inhibitor and the Fe(110) surface, directly influencing the corrosion inhibition performance. The results demonstrate that these inhibitor molecules are promising candidates for protecting iron surfaces from corrosion in acidic aqueous environments, showcasing their potential for practical applications in corrosion prevention.

The research revealed that p-cymene exhibited the most robust adsorption energy among the studied inhibitors, measuring approximately -5.318×10^6 kcal/mol. This result highlights that p-cymene forms the most potent bond with the Fe(110) surface, positioning it as the most efficient inhibitor for corrosion prevention. Conversely, cuminaldehyde displayed the weakest adsorption energy, signifying its lower effectiveness as an inhibitor.

In summary, the study establishes that the inhibitory performance of the investigated complexes follows the order of p-cymene > β -pinene > γ -terpinene > cuminaldehyde. These findings can potentially guide the development of more effective corrosion inhibitors for iron in acidic aqueous solutions, contributing to advancements in corrosion prevention strategies.

4. CONCLUSIONS

This scientific study rigorously explored the corrosion-inhibiting potential of cumin essential oil (EO) in a hydrochloric acid (HCl) environment, providing compelling evidence of its efficacy. Electrochemical techniques, specifically potentiodynamic polarization curves and electrochemical impedance spectroscopy (EIS), were employed to validate these findings. Notably, the inhibitory effect of cumin EO exhibited a direct correlation with its concentration, indicating its promising role in corrosion protection. Understanding the bonding interactions between the inhibitor molecule and the metal surface is pivotal to elucidating its inhibitory mechanism. The lowest unoccupied molecular orbital (LUMO) facilitates

electron transfer from the inhibitor to the metal, while the highest occupied molecular orbital (HOMO) enables back-donation of electrons from the metal to the inhibitor. Additionally, the Fermi energy of the metal, which dictates electron sharing between the metal and the inhibitor, further influences this interaction. Variations in the Fermi energy can impact the electron-transfer process and subsequently affect inhibitor–substrate bonding. Thus, a comprehensive understanding of the energetic positions of frontier orbitals and the metal's Fermi energy is essential for an accurate evaluation of inhibition efficiency. Visual examination of the steel surface exposed to a highly corrosive 0.5 M HCl medium revealed the formation of surface pits in the absence of the inhibitor. However, the introduction of cumin EO at a concentration of 2 g/L effectively formed a protective layer, shielding the steel from corrosion. This underscores the remarkable protective capacity of cumin EO even in harsh environments. Importantly, the study emphasizes the ecofriendliness of employing cumin EO as a green corrosion inhibitor, aligning with sustainable and environmentally conscious practices.

In summary, this study positions cumin EO as a potent and environmentally friendly solution for mitigating corrosion in mild steel exposed to acidic media. Its findings make a substantial contribution to corrosion science and provide a sustainable approach to safeguarding critical infrastructure and assets from the detrimental effects of corrosion.

AUTHOR INFORMATION

Corresponding Authors

Hana Ferkous – Département de Technologie, Université 20 août 1955 de Skikda, 21000 Skikda, Algeria; Laboratoire de Génie Mécanique et Matériaux, Faculté de Technologie, Université de 20 Août 1955, Skikda 21000, Algeria; Email: h.ferkous@univ-skikda.dz

Yacine Benguerba – Laboratoire de Biopharmacie Et Pharmaceutique (LPBT), Ferhat Abbas Setif 1 University, 19000 Setif, Algeria; orcid.org/0000-0002-8251-9724; Email: yacinebenguerba@univ-setif.dz

Authors

Aicha Rizi – Laboratory of Applied Organic Chemistry LCOA, Synthesis of Biomolecules and Molecular Modeling Group, Badji Mokhtar—Annaba University, Annaba 23000, Algeria

Amel Sedik – Scientific and Technical Research Center in Physico-chemical Analysis (CRAPC), RP 42004 Tipaza, Algeria

Anissa Acidi – Laboratory of Applied Organic Chemistry LCOA, Synthesis of Biomolecules and Molecular Modeling Group, Badji Mokhtar—Annaba University, Annaba 23000, Algeria

Khadidja Otmane Rachedi – Laboratory of Applied Organic Chemistry LCOA, Synthesis of Biomolecules and Molecular Modeling Group, Badji Mokhtar—Annaba University, Annaba 23000, Algeria

Malika Berredjem – Laboratory of Applied Organic Chemistry LCOA, Synthesis of Biomolecules and Molecular Modeling Group, Badji Mokhtar—Annaba University, Annaba 23000, Algeria

Amel Delimi – Département de Technologie, Université 20 août 1955 de Skikda, 21000 Skikda, Algeria; Laboratoire de Génie Mécanique et Matériaux, Faculté de Technologie, Université de 20 Août 1955, Skikda 21000, Algeria

Amdjed Abdennouri – Laboratoire de Physico-Chimie des Surfaces et des Interfaces, Université 20 août 1955 de Skikda, 21000 Skikda, Algeria

Manawwer ALAM – Department of Chemistry, College of Science, King Saud University, Riyadh 11451, Saudi Arabia; orcid.org/0000-0001-9540-8532

Barbara Ernst – Université de Strasbourg, CNRS, IPHC UMR 7178, Laboratoire de Reconnaissance et Procédés de Séparation Moléculaire (RePSeM), F-67000 Strasbourg, France

Complete contact information is available at:

<https://pubs.acs.org/10.1021/acsomega.3c06548>

Notes

The authors declare no competing financial interest.

ACKNOWLEDGMENTS

The authors gratefully acknowledge the funding from Researchers Supporting, Laboratory of Applied Organic Chemistry LCOA, Synthesis of Biomolecular and Molecular Modelling Group, Badji-Mokhtar-Annaba University, Box 12, 23000 Annaba, Algeria, Scientific and Technical Research Center in Physico-chemical Analysis (CRAPC), Laboratoire de Génie mécanique et Matériaux, Faculté de Technologie, University 20 Août 1955-Skikda, Skikda, 21000, Algeria, and the Ministry of Higher Education and Scientific Research, Ferhat ABBAS Setif 1 University, the Directorate General for Scientific Research and Technological Development (DGRSDT), Algeria. The authors are thankful to the Researchers Supporting Project (RSP2023R113), King Saud University, Riyadh, Saudi Arabia.

REFERENCES

- (1) Kaya, F.; Solmaz, R.; Geçibesler, İ. H. Adsorption and Corrosion Inhibition Capability of Rheum Ribes Root Extract (Işgın) for Mild Steel Protection in Acidic Medium: A Comprehensive Electrochemical, Surface Characterization, Synergistic Inhibition Effect, and Stability Study. *J. Mol. Liq.* **2023**, *372*, No. 121219.
- (2) Sedik, A.; Lerari, D.; Salci, A.; et al. Dardagan Fruit extract as eco-friendly corrosion inhibitor for mild steel in 1 M HCl: Electrochemical and surface morphological studies. *J. Taiwan Inst. Chem. Eng.* **2020**, *107*, 189–200.
- (3) Belakhdar, A.; Ferkous, H.; Djellali, S.; et al. Computational and experimental studies on the efficiency of Rosmarinus officinalis polyphenols as green corrosion inhibitors for XC48 steel in acidic medium. *Colloids Surf., A* **2020**, *606*, No. 125458.
- (4) Kahlouche, A.; Ferkous, H.; Delimi, A.; et al. Molecular insights through the experimental and theoretical study of the anticorrosion power of a new eco-friendly Cytisus multiflorus flowers extract in a 1 M sulfuric acid. *J. Mol. Liq.* **2022**, *347*, No. 118397.
- (5) Ferkous, H.; Zerroug, M.; Chaouch, M. A. et al. Green Corrosion Inhibitor for Carbon Steel in 1 M HCl: A Comparative Study of Polysaccharides Extracted from Prickly Pear Nopals of Opuntia Ficus-Indica (Peel and Pulp). In *Euro-Mediterranean Conference for Environmental Integration*; Springer, 2017.
- (6) Bowman, E.; Jacobson, G.; Koch, G.; et al. International measures of prevention, application, and economics of corrosion technologies study. *NACE Int.* **2016**, *216*, 2–3.
- (7) Shamsheera, K. O.; Prasad, A. R.; Arshad, M.; et al. A sustainable method of mitigating acid corrosion of mild steel using jackfruit pectin (JP) as green inhibitor: Theoretical and electrochemical studies. *J. Indian Chem. Soc.* **2022**, *99* (1), No. 100271, DOI: 10.1016/j.jics.2021.100271.
- (8) Belakhdar, A.; Ferkous, H.; Djellali, S. et al. Thermodynamic and Electrochemical Studies of Corrosion Inhibition of Carbon Steel by Rosmarinus Officinalis Extract in Acid Medium. In *Recent Advances in Environmental Science from the Euro-Mediterranean and Surrounding Regions*, 2nd ed.; Springer: Tunisia, 2021.
- (9) Meriem, Z.; Hana, F.; Souad, D.; et al. Experimental and theoretical evaluation of the adsorption process of some polyphenols and their corrosion inhibitory properties on mild steel in acidic media. *J. Environ. Chem. Eng.* **2021**, *9* (6), No. 106482.
- (10) Boukerche, S.; Ferkous, H.; Delimi, A.; et al. Anti-corrosion performance of dehydroacetic acid thiosemicarbazone on XC38 carbon steel in an acidic medium. *Arabian J. Chem.* **2023**, *16*, No. 105061.
- (11) Znini, M.; Majidi, L.; Bouyanzer, A.; et al. Essential oil of Salvia aucheri mesatlantica as a green inhibitor for the corrosion of steel in 0.5 M H₂SO₄. *Arabian J. Chem.* **2012**, *5* (4), 467–474.
- (12) Zerroug, M.; Ferkous, H.; Radjai, M. et al. An AFM Study of the Surface Propriety and Corrosion Inhibition on Carbon Steel in Acidic Media. In *Recent Advances in Environmental Science from the Euro-Mediterranean and Surrounding Regions*; Springer: Tunisia, 2018.
- (13) Sedik, A.; Abderrahmane, S.; Boukerche, S.; et al. Synergistic Effect of L-Methionine and KI on Copper Corrosion Inhibition in HNO₃ (1M). *Sens. Transducers* **2014**, *27*, 326–335.
- (14) Qiang, Y.; Zhang, S.; Guo, L.; et al. Experimental and theoretical studies of four allyl imidazolium-based ionic liquids as green inhibitors for copper corrosion in sulfuric acid. *Corros. Sci.* **2017**, *119*, 68–78.
- (15) Sedik, A.; Abderrahmane, S.; Himour, A. Cysteine inhibitor effects on copper corrosion in 1 M HNO₃ solution. *Sens. Lett.* **2011**, *9* (6), 2219–2222.
- (16) Djellali, S.; Ferkous, H.; Sahraoui, R. et al. Efficiency of Alkaloids Crude Extract of Cinnamomum Zeylanicum as Corrosion Inhibitor of Mild Steel in Sulfuric Acid Solution. In *Recent Advances in Environmental Science from the Euro-Mediterranean and Surrounding Regions*, 2nd ed.; Springer: Tunisia, 2021.
- (17) Ferkous, H.; Djellali, S.; Sahraoui, R. et al. Electrochemical Impedance Spectroscopy and Adsorption Study of Carbon Steel in 1 M HCl Solution Containing 2-(2-Methoxybenzylidene) Hydrazine-1-Carbothioamide. In *Recent Advances in Environmental Science from the Euro-Mediterranean and Surrounding Regions*, 2nd ed.; Springer: Tunisia, 2021.
- (18) Belakhdar, A.; Ferkous, H.; Djellali, S.; et al. Corrosion inhibition performance of Rosmarinus officinalis methanolic extract on carbon steel XC48 in acidic medium (2M HCl). *Mater. Biomater. Sci.* **2020**, *3* (2), No. 046-53.
- (19) Wang, X.; Yang, H.; Wang, F. An investigation of benzimidazole derivative as corrosion inhibitor for mild steel in different concentration HCl solutions. *Corros. Sci.* **2011**, *53* (1), 113–121.

- (20) Gupta, N. K.; Joshi, P. G.; Srivastava, V.; et al. Chitosan: A macromolecule as green corrosion inhibitor for mild steel in sulfamic acid useful for sugar industry. *Int. J. Biol. Macromol.* **2018**, *106*, 704–711.
- (21) Boulechfar, C.; Ferkous, H.; Djellali, S.; et al. DFT/molecular scale, MD simulation and assessment of the eco-friendly anti-corrosion performance of a novel Schiff base on XC38 carbon steel in acidic medium. *J. Mol. Liq.* **2021**, *344*, No. 117874.
- (22) Ostovari, A.; Hoseinie, S. M.; Peikari, M.; et al. Corrosion inhibition of mild steel in 1 M HCl solution by henna extract: A comparative study of the inhibition by henna and its constituents (Lawson, Gallic acid, α -D-Glucose and Tannic acid). *Corros. Sci.* **2009**, *51* (9), 1935–1949.
- (23) Ferkous, H.; Zerroug, M.; Radjai, M. et al. Electrochemical and Surface Morphological Studies of a Carbon Steel Corrosion by Natural Product in Acidic Solution. In *Recent Advances in Environmental Science from the Euro-Mediterranean and Surrounding Regions*; Springer: Tunisia, 2018.
- (24) Madaci, A.; Ferkous, H.; Sedik, A.; et al. Experimental and theoretical study of polysaccharides extracted from prickly pear nopales Pulp (PPUN) of *Opuntia ficus-indica* as corrosion inhibitors. *J. Mol. Liq.* **2023**, *384*, No. 122272.
- (25) Acidi, A.; Sedik, A.; Rizi, A.; et al. Examination of the main chemical components of essential oil of *Syzygium aromaticum* as a corrosion inhibitor on the mild steel in 0.5 M HCl medium. *J. Mol. Liq.* **2023**, *391*, No. 123423.
- (26) Shalabi, K.; Abdel-Galil, E.; El-Askalany, A. H.; et al. Adsorption, electrochemical behavior, and theoretical studies for copper corrosion inhibition in 1 M nitric acid medium using triazine derivatives. *J. Mol. Liq.* **2022**, *348*, No. 118420.
- (27) Thakur, A.; Kaya, S.; Abousalem, A. S.; et al. Computational and experimental studies on the corrosion inhibition performance of an aerial extract of *Cnicus Benedictus* weed on the acidic corrosion of mild steel. *Process Saf. Environ. Prot.* **2022**, *161*, 801–818.
- (28) Van de Vel, E.; Sampers, I.; Raes, K. A review on influencing factors on the minimum inhibitory concentration of essential oils. *Crit. Rev. Food Sci. Nutr.* **2019**, *59* (3), 357–378.
- (29) Bathily, M.; Ngom, B.; Gassama, D.; et al. Review on essential oils and their corrosion-inhibiting properties. *Am. J. Appl. Chem.* **2021**, *9* (3), 65–73.
- (30) Dahmani, K.; Galai, M.; Ouakki, M.; et al. Quantum chemical and molecular dynamic simulation studies for the identification of the extracted cinnamon essential oil constituent responsible for copper corrosion inhibition in acidified 3.0 wt% NaCl medium. *Inorg. Chem. Commun.* **2021**, *124*, No. 108409.
- (31) Mzioud, K.; Habsaoui, A.; Ouakki, M.; et al. Inhibition of copper corrosion by the essential oil of *Allium sativum* in 0.5 M H₂SO₄ solutions. *SN Appl. Sci.* **2020**, *2*, No. 1611.
- (32) Houbairi, S.; Lamiri, A.; Essahli, M. Corrosion Inhibition of Copper in 2M HNO₃ using the Essential Oil *Eugenia caryophyllus*. *Chem. Sci. Rev. Lett.* **2011**, *311*, 353–366.
- (33) Nadia, B.; Fayçal, D.; Imad, E. H.; et al. Gravimetric, Electrochemical, and Surface Morphological Studies of *Ammodaucus Lecotrichus* Essential Oil as Corrosion Inhibitor for Copper Surface in Hydrochloric Acid Medium. *Anal. Bioanal. Electrochem.* **2021**, *13* (3), 340–357.
- (34) Houbairi, S. et al. Study of the inhibitory activity of the essential oil of *Myrtus communis* against copper corrosion in a nitric acid medium, 2015.
- (35) El-Asri, A.; Rguiti, M.; Jmiai, A.; et al. Carissa macrocarpa extract (ECM) as a new efficient and ecologically friendly corrosion inhibitor for copper in nitric acid: Experimental and theoretical approach. *J. Taiwan Inst. Chem. Eng.* **2023**, *142*, No. 104633.
- (36) Samal, P. P.; Singh, C. P.; Krishnamurthy, S. Expounding lemonal terpenoids as corrosion inhibitors for copper using DFT based calculations. *Appl. Surf. Sci.* **2023**, *614*, No. 156066.
- (37) Halambek, J.; Žutinić, A.; Berković, K. *Ocimum basilicum* L. oil as corrosion inhibitor for aluminium in hydrochloric acid solution. *Int. J. Electrochem. Sci.* **2013**, *8* (9), 11201–11214.
- (38) Uwineza, M. S.; Essahli, M.; Lamiri, A. Corrosion inhibition of aluminium in 2 M phosphoric acid using the essential oil of mentha pulegium leaves. *Port. Electrochim. Acta* **2016**, *34* (1), 53–62.
- (39) Sanni, O.; Iwarere, S. A.; Daramola, M. O. Evaluation of Corrosion Inhibition of Essential Oil-Based Inhibitors on Aluminum Alloys. *ACS Omega* **2022**, *7* (45), 40740–40749.
- (40) Halambek, J.; Bubalo, M. C.; Redovnikovic, I. R.; et al. Corrosion behaviour of aluminium and AA5754 alloy in 1% acetic acid solution in presence of laurel oil. *Int. J. Electrochem. Sci.* **2014**, *9* (10), 5496–5506.
- (41) Ennouri, A.; Essahli, M.; Lamiri, A. Corrosion Inhibition of Aluminum in Hydrochloric Acid Medium by Essential Oil of *Eucalyptus camaldulensis* and *Myrtus Communis*. **2019**, *11*, 913–929.
- (42) Sanni, O.; Popoola, A.; Fayomi, O. Oil as corrosion inhibitor for aluminium alloy in aggressive environment. *IOP Conf. Ser.: Mater. Sci. Eng.* **2018**, *391*, No. 012004, DOI: 10.1088/1757-899x/391/1/012004.
- (43) Loto, R. T.; Mbah, E. H.; Ugada, J. I. Corrosion inhibition effect of citrus sinensis essential oil extract on plain carbon steel in dilute acid media. *S. Afr. J. Chem. Eng.* **2021**, *35*, 159–164.
- (44) Abdallah, M.; Altass, H.; Al-Gorair, A. S.; et al. Natural nutmeg oil as a green corrosion inhibitor for carbon steel in 1.0 M HCl solution: Chemical, electrochemical, and computational methods. *J. Mol. Liq.* **2021**, *323*, No. 115036.
- (45) Marciales, A.; Haile, T.; Ahvazi, B.; et al. Performance of green corrosion inhibitors from biomass in acidic media. *Corros. Rev.* **2018**, *36* (3), 239–266.
- (46) Manssouri, M.; Znini, M.; Lakbaibi, Z.; et al. Experimental and computational studies of perillaldehyde isolated from *Ammodaucus leucotrichus* essential oil as a green corrosion inhibitor for mild steel in 1.0 M HCl. *Chem. Pap.* **2021**, *75*, 1103–1114.
- (47) Boumhara, K.; Tabyaoui, M.; Jama, C.; et al. *Artemisia Mesatlantica* essential oil as green inhibitor for carbon steel corrosion in 1 M HCl solution: Electrochemical and XPS investigations. *J. Ind. Eng. Chem.* **2015**, *29*, 146–155.
- (48) El-Sawi, S. A.; Mohamed, M. Cumin herb as a new source of essential oils and its response to foliar spray with some microelements. *Food Chem.* **2002**, *77* (1), 75–80.
- (49) Koffi, A. A.; Muralidharan, S.; Trokourey, A. Corrosion inhibition of carbon steel using extract of *Mussaenda erythrophylla* leaves: interfacial action mode in sulfuric acid medium/Inhibition de la corrosion de l'acier à l'aide d'extrait de feuilles de *Mussaenda erythrophylla*: mode d'action interfaciale en milieu acide sulfurique. *J. Soc. Ouest-Afr. Chim.* **2015**, *40*, No. 31.
- (50) Shalabi, K.; Nazeer, A. A. Adsorption and inhibitive effect of *Schinus terebinthifolius* extract as a green corrosion inhibitor for carbon steel in acidic solution. *Prot. Met. Phys. Chem. Surf.* **2015**, *51*, 908–917.
- (51) Fouda, A. S.; Abousalem, A. S.; El-Ewady, G. Y. Mitigation of corrosion of carbon steel in acidic solutions using an aqueous extract of *Tilia cordata* as green corrosion inhibitor. *Int. J. Ind. Chem.* **2017**, *8*, 61–73.
- (52) Prabakaran, M.; Kim, S. H.; Sasireka, A.; et al. *Polygonatum odoratum* extract as an eco-friendly inhibitor for aluminum corrosion in acidic medium. *J. Adhes. Sci. Technol.* **2018**, *32* (18), 2054–2069.
- (53) Gabsi, M.; Ferkous, H.; Delimi, A.; et al. The curious case of polyphenols as green corrosion inhibitors: a review on their extraction, design, and applications. *Environ. Sci. Pollut. Res.* **2023**, *30*, 59081–59105.
- (54) Radjai, M.; Ferkous, H.; Zerroug, M.; Djellali, S. et al. Methanolic Extract of *Artemisia Herba Alba* as Eco-Friendly Inhibitor of Carbon Steel Corrosion in 1M HCl Media. In *Recent Advances in Environmental Science from the Euro-Mediterranean and Surrounding Regions*; Springer: Tunisia, 2018.
- (55) El Hajjaji, F.; Greche, H.; Taleb, M.; et al. Application of essential oil of thyme vulgaris as green corrosion inhibitor for mild steel in 1 M HCl. *J. Mater. Environ. Sci.* **2016**, *7* (2), 567–578.

- (56) Chetouani, A.; Hammouti, B. *Salvia officinalis* essential oil and the extract as green corrosion inhibitor of mild steel in hydrochloric acid. *J. Chem. Pharm. Res.* **2014**, *6*, 1401–1416.
- (57) Ferkous, H.; Rouibah, K.; Hammoudi, N. E. H.; et al. The removal of a textile dye from an aqueous solution using a biocomposite adsorbent. *Polymers* **2022**, *14* (12), No. 2396.
- (58) Behloul, H.; Ferkous, H.; Bougdah, N.; et al. New insights on the adsorption of CI-Reactive Red 141 dye using activated carbon prepared from the ZnCl₂-treated waste cotton fibers: Statistical physics, DFT, COSMO-RS, and AIM studies. *J. Mol. Liq.* **2022**, *364*, No. 119956.
- (59) Delimi, A.; Ferkous, H.; Alam, M.; et al. Corrosion protection performance of silicon-based coatings on carbon steel in NaCl solution: a theoretical and experimental assessment of the effect of plasma-enhanced chemical vapor deposition pretreatment. *RSC Adv.* **2022**, *12* (24), 15601–15612.
- (60) Sedik, A.; Athmani, S.; Saoudi, A.; et al. Experimental and theoretical insights into copper corrosion inhibition by protonated amino-acids. *RSC Adv.* **2022**, *12* (36), 23718–23735.
- (61) Boulechfar, C.; Ferkous, H.; Boufas, S.; et al. Synthesis, electrochemical, and quantum chemical studies of some metal complexes: Mn (II), Co (II), and Zn (II) with 2-furaldehyde semicarbazone. *J. Mol. Struct.* **2023**, *1271*, No. 134007.
- (62) Rouibah, K.; Ferkous, H.; Delimi, A.; et al. Biosorption of zinc (II) from synthetic wastewater by using *Inula Viscosa* leaves as a low-cost biosorbent: Experimental and molecular modeling studies. *J. Environ. Manage.* **2023**, *326*, No. 116742.
- (63) Fakhry, H.; El Faydy, M.; Benhiba, F.; et al. Experimental, DFT studies and molecular dynamic simulation on the corrosion inhibition of carbon steel in 1 M HCl by two newly synthesized 8-hydroxyquinoline derivatives. *J. Indian Chem. Soc.* **2022**, *99* (12), No. 100701.
- (64) Boudjelida, S.; Djellali, S.; Ferkous, H.; et al. Physicochemical Properties and Atomic-Scale Interactions in Polyaniline (Emeraldine Base)/Starch Bio-Based Composites: Experimental and Computational Investigations. *Polymers* **2022**, *14* (8), No. 1505.
- (65) Siğircik, G.; Tüken, T.; Erbil, M. Assessment of the inhibition efficiency of 3, 4-diaminobenzonitrile against the corrosion of steel. *Corros. Sci.* **2016**, *102*, 437–445.
- (66) Ferreira, E.; Giacomelli, C.; Giacomelli, F. C.; et al. Evaluation of the inhibitor effect of L-ascorbic acid on the corrosion of mild steel. *Mater. Chem. Phys.* **2004**, *83* (1), 129–134.
- (67) Ferkous, H.; Djellali, S.; Sahraoui, R. et al. 2-(2-Methoxybenzylidene) Hydrazine-1-Carbothioamide as Efficient Organic Inhibitor for Mild Steel in Hydrochloric Acid Solution. In *Recent Advances in Environmental Science from the Euro-Mediterranean and Surrounding Regions*, 2nd ed.; Springer: Tunisia, 2021.
- (68) Ferkous, H.; Djellali, S.; Sahraoui, R.; et al. Corrosion inhibition of mild steel by 2-(2-methoxybenzylidene) hydrazine-1-carbothioamide in hydrochloric acid solution: Experimental measurements and quantum chemical calculations. *J. Mol. Liq.* **2020**, *307*, No. 112957.
- (69) Yilmaz, N.; Fitoz, A.; Ergun, Y.; Emregül, K. C. A combined electrochemical and theoretical study into the effect of 2-((thiazole-2-ylimino) methyl) phenol as a corrosion inhibitor for mild steel in a highly acidic environment. *Corros. Sci.* **2016**, *111*, 110–120.
- (70) Solmaz, R.; Salcı, A.; Dursun, Y. A.; et al. A comprehensive study on the adsorption, corrosion inhibition efficiency and stability of acriflavine on mild steel in 1 M HCl solution. *Colloids Surf., A* **2023**, *674*, No. 131908.
- (71) Al-Moubaraki, A. H.; Al-Judaibi, A.; Asiri, M. Corrosion of C-steel in the Red Sea: Effect of immersion time and inhibitor concentration. *Int. J. Electrochem. Sci.* **2015**, *10* (5), 4252–4278.
- (72) Ahmed, R. A. Investigation of corrosion inhibition of vitamins B1 and C on mild steel in 0.5 M HCl solution: experimental and computational approach. *Orient. J. Chem.* **2016**, *32* (1), No. 295.
- (73) Al-Fahemi, J. H.; Abdallah, M.; Gad, E. A. M.; et al. Experimental and theoretical approach studies for melatonin drug as safely corrosion inhibitors for carbon steel using DFT. *J. Mol. Liq.* **2016**, *222*, 1157–1163.
- (74) Al-Moubaraki, A. H.; Chaouiki, A.; Alahmari, J. M.; et al. Development of Natural Plant Extracts as Sustainable Inhibitors for Efficient Protection of Mild Steel: Experimental and First-Principles Multi-Level Computational Methods. *Materials* **2022**, *15* (23), No. 8688.
- (75) Tantawy, A. H.; Soliman, K. A.; El-Lateef, H. M. A. Novel synthesized cationic surfactants based on natural piper nigrum as sustainable-green inhibitors for steel pipeline corrosion in CO₂-3.5% NaCl: DFT, Monte Carlo simulations and experimental approaches. *J. Cleaner Prod.* **2020**, *250*, No. 119510.
- (76) Zhang, W.; Ma, Y.; Chen, L.; et al. Aloe polysaccharide as an eco-friendly corrosion inhibitor for mild steel in simulated acidic oilfield water: Experimental and theoretical approaches. *J. Mol. Liq.* **2020**, *307*, No. 112950.
- (77) Mendonça, G. L. F.; Costa, S. N.; Freire, V. N.; Casciano, P. N. S.; et al. Understanding the corrosion inhibition of carbon steel and copper in sulphuric acid medium by amino acids using electrochemical techniques allied to molecular modelling methods. *Corros. Sci.* **2017**, *115*, 41–55.
- (78) Saraswat, V.; Yadav, M.; Obot, I. B. Investigations on eco-friendly corrosion inhibitors for mild steel in acid environment: Electrochemical, DFT and Monte Carlo Simulation approach. *Colloids Surf., A* **2020**, *599*, No. 124881.
- (79) Ahmed, M. H. O.; Al-Amieri, A. A.; Al-Majedy, Y. K.; et al. Synthesis and characterization of a novel organic corrosion inhibitor for mild steel in 1 M hydrochloric acid. *Results Phys.* **2018**, *8*, 728–733.
- (80) Balasubramani, S. G.; Chen, G. P.; Coriani, S.; et al. TURBOMOLE: Modular program suite for ab initio quantum-chemical and condensed-matter simulations. *J. Chem. Phys.* **2020**, *152* (18), No. 184107.
- (81) Damej, M.; Skal, S.; Aslam, J.; et al. An environmentally friendly formulation based on Cannabis sativa L. seed oil for corrosion inhibition of E24 steel in HCl medium: Experimental and theoretical study. *Colloids Surf., A* **2022**, *643*, No. 128745.
- (82) Rachedi, K. O.; Bahadi, R.; Aissaoui, M.; et al. DFT Study, POM analyses and molecular docking of novel oxazaphosphinanes: Identification of antifungal pharmacophore site. *Indones. J. Chem.* **2020**, *20* (2), 440–450.
- (83) Rachedi, K. O.; Ouk, T.-S.; Bahadi, R.; Bouzina, A.; et al. Synthesis, DFT and POM analyses of cytotoxicity activity of α -amidophosphonates derivatives: Identification of potential antiviral O, O-pharmacophore site. *J. Mol. Struct.* **2019**, *1197*, 196–203.
- (84) Chetouani, A.; Hammouti, B. *Salvia officinalis* essential oil and the extract as green corrosion inhibitor of mild steel in hydrochloric acid. *J. Chem. Pharm. Res.* **2014**, *6* (7), 1401–1416.